Article

Control of the Photo-Isomerization Mechanism in 3*H*-Naphthopyrans to Prevent Formation of Unwanted Long-Lived Photoproducts

Sabina Brazevic [1], Stanisław Nizinski [1], Michel Sliwa [2], Jiro Abe [3,*], Michał F. Rode [4,*] and Gotard Burdzinski [1,*]

[1] Faculty of Physics, Adam Mickiewicz University in Poznan, Uniwersytetu Poznanskiego 2, 61-614 Poznan, Poland; sabina.brazevic@amu.edu.pl (S.B.); stanislaw.nizinski@amu.edu.pl (S.N.)

[2] Laboratoire de Spectroscopie pour les Interactions, la Réactivité et l'Environnement, LASIRE, CNRS, UMR 8516, Univ. Lille, 59000 Lille, France; michel.sliwa@univ-lille.fr

[3] Department of Chemistry, School of Science and Engineering, Aoyama Gakuin University, 5-10-1 Fuchinobe, Chuo-ku, Sagamihara, Kanagawa 252-5258, Japan

[4] Institute of Physics, Polish Academy of Sciences, Aleja Lotników 32/46, 02-668 Warsaw, Poland

* Correspondence: jiro_abe@chem.aoyama.ac.jp (J.A.); mrode@ifpan.edu.pl (M.F.R.); gotardb@amu.edu.pl (G.B.)

check for
updates

Abstract: In the photochromic reactions of 3*H*-naphthopyrans, two colored isomers TC (transoid-*cis*) and TT (transoid-*trans*) are formed. In terms of optimized photo-switchable materials, synthetic efforts are nowadays evolving toward developing 3*H*-naphthopyran derivatives that would not be able to photoproduce the long-living transoid-*trans*, TT, photoproduct. The substitution with a methoxy group at position 10 results in significant reduction of the TT isomer formation yield. The TC photophysics responsible for TT suppression were revealed here using a combination of multi-scale time resolved absorption UV-vis spectroscopy and ab initio calculations. The substitution changes the TC excited-state potential energy landscape, the *bicycle-pedal* isomerization path is favored over the rotation around a single double bond. The *bicycle-pedal* path is aborted in halfway to TT formation due to $S_1 \rightarrow S_0$ internal conversion populating back the TC species in the ground electronic state. This is validated by a shorter TC S_1 state lifetime for methoxy derivative in comparison to that of the parent-unsubstituted compound (0.47 ± 0.05 ps vs. 0.87 ± 0.09 ps) in cyclohexane.

1. Introduction

Discovery of photochromic chromenes by Becker and Michl in 1966 initiated numerous studies related to their fundamental characterization and applications, especially as photochromic lenses [1]. One of the most frequently studied compounds belonging to this family is 3,3-diphenyl-3*H*-naphtho[2,1-*b*]pyran (see Scheme 1, CF-H, also known as 2,2-diphenyl-5,6-benzo(2*H*)chromene) [1–21].

The coloration process in this molecule—which is based on the photoinduced opening of the pyran ring in its closed form (CF)—is ultrafast as it takes place on a few ps time-scale leading to the transoid-*cis* TC form (see Scheme 1) [3,11,14,22–25]. In the next step transoid-*trans* TT form is produced by TC photoexcitation or is formed as a direct product of the pyran ring-opening [12,17]. A serious drawback of 3*H*-naphthopyran family is the long fading time of the transoid-*trans* TT isomer. While the TC form relaxes over tens of seconds, the persistence of the long-lived TT form over hours is a limiting factor for classical applications such as photochromic lenses, due to inconvenient slow fading

response to UV light switch off. Thus, recent research has been focused on minimization of the TT formation yield in the photoreaction by designing new 3*H*-naphthopyran derivatives with appropriate substituents [21,22,26,27]. Aryl substituents in position 2 of 3*H*-naphthopyrans can exert both steric and electrostatic repulsion effects which have been suggested to suppress TT formation [22]. Exceptionally short TC lifetime, on the order of tens of microseconds in solution, make TC→TT photoisomerization inefficient upon stationary UV irradiation. However in this case, the photostationary formation yield of TC is also low. Keeping the TC lifetime of seconds and the suppression of the TT formation have been recently reported for 3*H*-naphthopyran with methoxy group substitution at position 10 (CF-OCH$_3$, see Scheme 1) [21]. It has been proposed that the alkoxy group effectively reduces the formation of the transoid-*trans* form due to C−H···O intramolecular hydrogen bonding in the TC form [21]. The mechanism of TT suppression requires detailed studies of TC excited-state energy landscape.
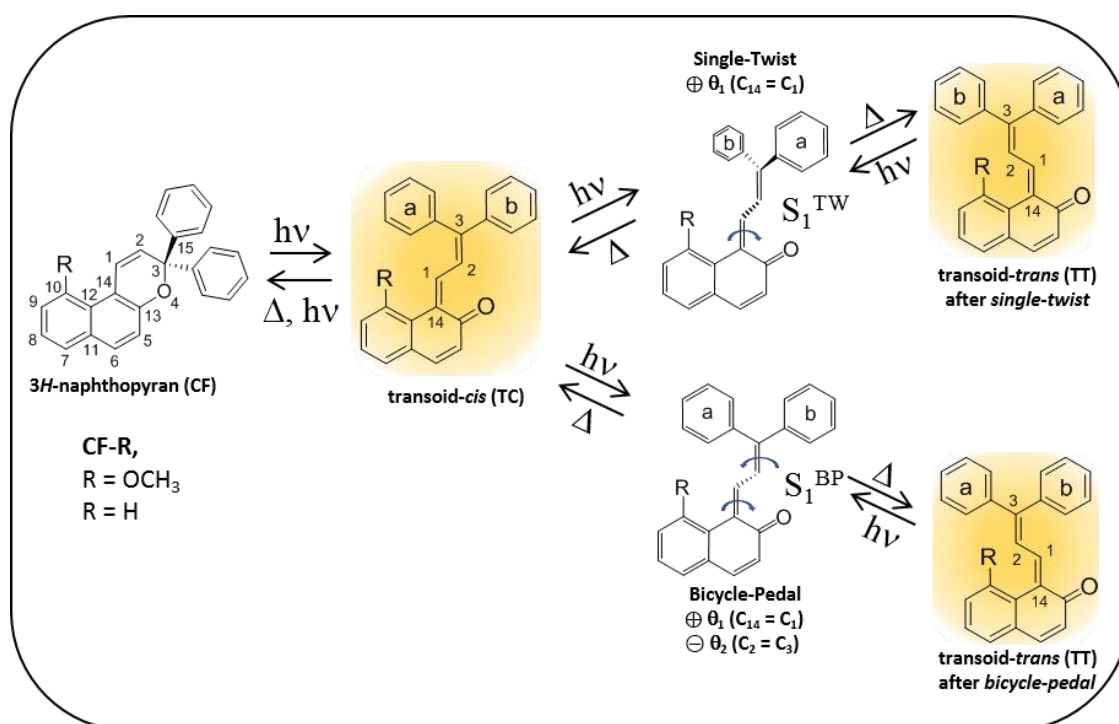
Scheme 1. Two mechanistic pathways of the TC→TT photoisomerization process; the *single-twist* vs. *bicycle-pedal* motion. The presence of the methoxy group in 10-methoxy-CF (CF-OCH$_3$) reduces the yield of the TT isomer formation [21]. θ_1(C$_{14}$ = C$_1$) and θ_2(C$_2$ = C$_3$) are two driving coordinates defined by the rotation about C$_{13}$−C$_{14}$=C$_1$−C$_2$ and C$_1$−C$_2$=C$_3$−C$_{15}$ dihedral angles, respectively.

Recently we have reinvestigated TT formation mechanism for unsubstituted 3*H*-naphthopyran (CF-H). We have shown that TC→TT photoisomerization competes with the other deactivation channels such as: S$_1$→S$_0$ internal conversion (major), S$_1$→T$_1$ intersystem crossing, S$_1$ state fluorescence and allenyl-naphthol AP formation (hydrogen shift reaction) [25]. With this knowledge, we undertook comprehensive experimental and theoretical studies to explain why the presence of a methoxy group at position 10 of 3*H*-naphthopyran can so dramatically decrease the yield of TC→TT photoreaction. We apply multi-scale (from hundreds of femtoseconds to seconds) UV-vis time resolved absorption spectroscopy and quantum chemical calculations for 3*H*-naphthopyrans: CF-H and CF-OCH$_3$. We have shown here for the first time two isomerization mechanisms TC→TT: (i) sole double bond isomerization with a *single-twist* competing with (ii) a *bicycle-pedal* isomerization (Scheme 1). The latter one is the dominant pathway for TC-OCH$_3$ while the single-twist is the main one for TC-H. In the case of *bicycle-pedal* mechanism, isomerization is aborted in halfway to TT. Altogether, the *bicycle-pedal* has

been shown a photostabilizing channel for TC form, thus this pathway plays a key role to effectively reduce TT concentration in the photoreaction.

2. Results and Discussion

2.1. The Effect of Methoxy Group Presence on the Ground-State Energy Landscape and the UV Absorption Spectrum

As far as the UV absorption spectrum is concerned, the calculations for CF-OCH$_3$ molecule predict a very slight red-shift of the absorption maximum, in comparison to its position for the model chromene (CF-H), which in energy scale is not higher than 0.1 eV. This is in excellent agreement with experiment which gives the maximum of absorption at 361 nm in cyclohexane (3.44 eV) for CF-H [28] and 370 nm (3.35 eV) for CF-OCH$_3$ (Figure S1). The observed red-shift is the effect of H substitution with a π-electron donating group, O−CH$_3$, that decreases the excitation energy value of all the S$_0$→S$_n$(ππ*) electron transitions in CF. Such behavior has been observed earlier for methoxy substituted 3*H*-naphthopyrans (6-, 7- and 8-methoxy derivatives) [5,29].

3*H*-Naphthopyrans typically produce both TC and TT isomers (see Scheme 1) under conditions of continuous UV irradiation tuned to the CF absorption band. These TC and TT isomers are structurally related through the rotation about the C$_{13}$−C$_{14}$=C$_1$−C$_2$ dihedral angle. The UV absorption spectra of TC and TT are then quite similar (see Tables S1 and S2) since the π-electron conjugation in those two forms is alike. Even though, in both forms the strongest S$_0$→S$_2$ transition is slightly red shifted for TC relative to its position for TT (Figure 1b). The methoxy group substitution does not change much the chromene's ground-state energy landscape (calculated at the MP2/cc-pVDZ theory level) leaving the S$_0$-state energy barriers almost unchanged [28]. Thus, similarly as in the H counterpart, TC-OCH$_3$ and TT-OCH$_3$ forms do not differ much energetically. The difference between the relative energies of the respective H and OCH$_3$ derivatives is marginal, less than 0.02 eV, and both forms lie much above the closed-pyran form CF, app. by + 0.6 eV.
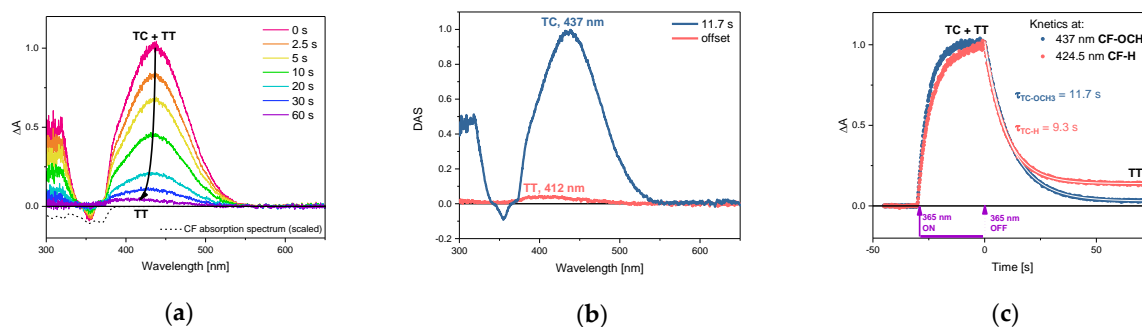

| (a) | (b) | (c) |

Figure 1. (**a**) UV-vis transient absorption spectra recorded for a solution of CF-OCH$_3$ in cyclohexane (c ≈ 1 × 10^{-4} M) at 21 °C after turning off LED UV irradiation at 365 nm (5 mW/cm^2); (**b**) Global analysis results in DAS (decay associated spectra) and two characteristic components: 11.7 s (TC lifetime) and the offset (TT); (**c**) Comparison of kinetics traces at 437 nm and 424.5 nm recorded for CF-OCH$_3$ and CF-H respectively.

2.2. TT Formation, Single-vs. Two-Photon Mechanism

To unmix TT and TC contribution at the photo-stationary state under UV irradiation, the usual method is to follow thermal recovery to CF. Indeed after the decay of TC, only TT form remains. Figure 1a shows then time evolution of transient absorption spectra recorded for CF-OCH$_3$ in cyclohexane after switching off UV irradiation (experimental set-up in Scheme S1). The initial absorption band corresponds to the mixture of TC (major) and TT (minor) species.

Figure 1b shows that the absorption maximum of TC-OCH$_3$ occurs at 437 nm (2.84 eV), while that of TT-OCH$_3$ isomer at 412 nm (3.01 eV), in cyclohexane (compare expt. vs theory in Table S1),

corresponding to the spectral locations for H-derivative (427 nm, for TC-H, and 412 nm, for TT-H, Table S2). The TC lifetime is slightly longer for the methoxy form (11.7 s vs. 9.3 s in cyclohexane, see Table 1). A polar solvent as acetonitrile stabilizes the TC-OCH_3 species (lifetime 17.0 s), indeed calculations show a substantial dipole moment of 4.2 D (Table S1). Figure 1c shows that TT isomer in cyclohexane is formed in smaller amount from CF-OCH_3 than from CF-H precursor, in agreement with the data reported by Inagaki et al. [21]. On the basis of DAS amplitudes selected at the TT and TC maxima we estimate that CF-OCH_3 in relation to CF-H described recently [25], produces four times less TT form under the same experimental conditions. Two parallel reaction mechanisms leading to TT isomer have been considered in literature [12,17]. One is a two-photon absorption process:

$$CF \xrightarrow{365 \text{ nm}} TC \xrightarrow{365 \text{ nm}} TT$$

while the second one is a single photon excitation path:

$$CF \xrightarrow{365 \text{ nm}} TT$$

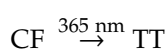**Table 1.** Photophysical properties of TC in solution: S_0 and S_1 absorption band maxima, lifetime τ_{S0} and excited state lifetime τ_{S1}.

Compound	Solvent	S_0(TC) λ_{abs}^{max}	τ_{S0}, s	S_1(TC) λ_{abs}^{max}	τ_{S1}, ps
TC-OCH_3	cyclohexane	437 nm	11.7 [1]	525 nm [3]	0.47 [2]
	acetonitrile	447 nm	17.0 [1]	545 nm	0.27 [2]
TC-H	cyclohexane	427 nm	9.3 [1]	520 nm [3]	0.87 [2]
	acetonitrile	430 nm	8.6 [1]	513 nm	0.31 [2]

Temperature: [1] 21 °C; Accuracy: [1] ± 5%; [2] ± 10%; τ_{S1} retrieved from band integral kinetics; [3] in agreement with calculations (Tables S3 and S4, respectively).

Experiments performed for CF-H to characterize the influence of the UV irradiation power on the TT absorbance signal (Figure 2a) show the slope of this relation to be 1.5 in agreement with reported data [28]. The slope value close to 2 is expected for a purely biphotonic process. The discrepancy can be explained by a small contribution of the single-photon reaction, additionally to the main consecutive two-photon absorption reaction path. We performed numerical simulations (see SI for details) for CF-H in cyclohexane using photophysical properties determined recently [28] that quantify for the first time the yields of both processes. A quantum yield of 0.003 for the single-photon channel explains the experimental data (Figure 2b, the slope of 1.5). The single photon process leading to TT has intriguing nature, since it requires the initial ring-opening followed by significant changes in geometry, which contradicts the intuition. However, one can expect that upon ring-opening process TC form is initially generated in the vibrationally excited state. Such excess of vibrational energy can lead the hot TC molecule to overcome relatively high (~1.2 eV) S_0-state energy barrier to form TT isomer.

The experimental slope determined for CF-OCH_3 is closer to unity (1.2, Figure 2a), which indicates a greater contribution of the single photon excitation path in the TT-OCH_3 formation (CF→TT) that correlates to a lower TT-OCH_3 signal level. The reason for the decrease in the share of biphotonic channel (CF→TC→TT) is linked to the photo-dynamics of TC-OCH_3 and needs thus to be determined precisely.
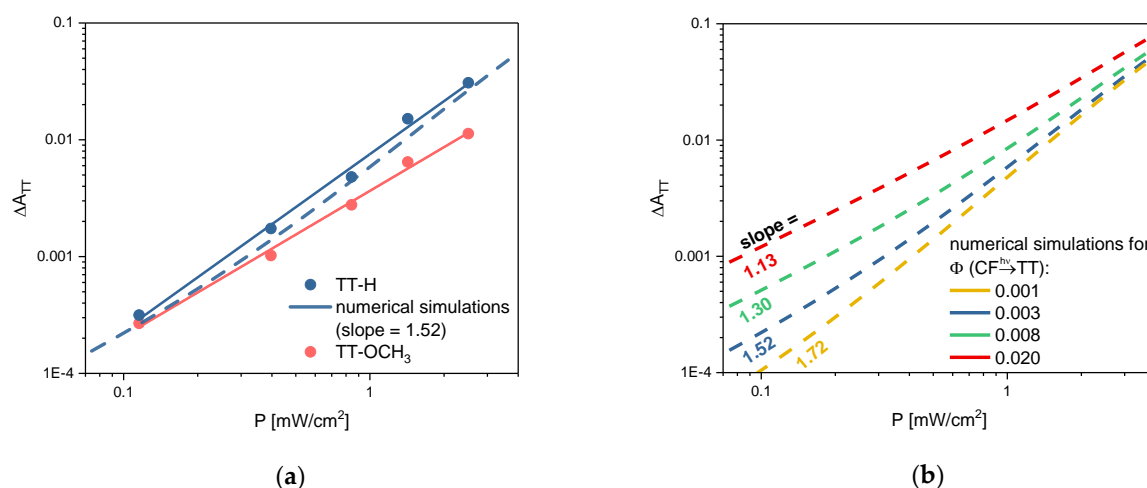
(**a**)   (**b**)

Figure 2. UV irradiation of CF in cyclohexane at 365 nm (3.40 eV) leads to TT population. (**a**) Plot of the TT absorption signal dependence on UV intensity on a log–log scale. The blue and red solid lines with slopes of 1.5 for TT-H and 1.2 for TT-OCH$_3$, respectively, are the best linear fit to the observed data. (**b**) Numerical simulations for TT-H traced for various yields Φ of the direct single photon excitation path CF $\overset{h\upsilon}{\rightarrow}$ TT.

2.3. Photophysical Properties of TC-OCH$_3$ in the Singlet Excited State

Ultrafast transient UV-vis absorption experiments were performed for TC-OCH$_3$ in cyclohexane with photoexcitation at 475 nm (2.61 eV). In these experiments, a solution of CF-OCH$_3$ was under a continuous LED UV irradiation at 365 nm (3.40 eV) to ensure a constant TC-OCH$_3$ concentration. Although TT is also produced, its concentration is over 20 times lower than that of TC. Moreover the selected pump excitation wavelength at 475 nm (2.61 eV) favors TC excitation over TT on the basis of the respective absorption band locations (Figure 1b). Thus, the measured transient absorption spectra can be securely assigned to the sole excitation of TC-OCH$_3$. Figure 3a shows the evolution of the transient absorption bands, which resemble the data reported for TC-H [25]. The initial positive transient absorption band peaking at 525 nm (2.36 eV) corresponds to TC-OCH$_3$ in the singlet excited state (S$_1$→S$_n$), which is in agreement with theoretical calculations (Table S3). The band undergoes a substantial decay (88%) in the time window 0.3–2 ps which is concomitant with the recovery of the negative band peaking at 435 nm. The negative band corresponds to the depopulation band, i.e., depletion of the TC-OCH$_3$ in the S$_0$ state caused by laser pulse excitation at 475 nm (2.61 eV). The global analysis indicates two characteristic time-constants (see Figure 3b): 0.45 ps - related to the lifetime τ_{S1} of TC-OCH$_3$ in the S$_1$ state, and 5.1 ps corresponding to the vibrationally hot S$_0$ species produced by S$_1$→S$_0$ internal conversion. The lifetime τ_{S1} can be also obtained from analysis of the band integral kinetics (0.47 ± 0.05 ps, Figure S2). The offset shows a weak positive band at 535 nm (2.32 eV) (see the offset × 15 in Figure 3b), which is assigned to the triplet excited state T$_1$ produced by intersystem crossing S$_1$→T$_1$ as in the parent TC-H compound [25].

A significant shortening of singlet excited state lifetime for the methoxy TC derivative in comparison to the H-parent compound (0.47 vs. 0.87 ps) is observed in cyclohexane (Table 1).

Moreover, data comparison at 50 ps delay (Figure 3a) shows less pronounced S$_0$ depopulation. Both observations can be explained by a more effective S$_1$→S$_0$ internal conversion channel in TC-OCH$_3$ compound that rationalizes the decrease in TT formation in two photon process and then lower TT concentration in the photostationary state in comparison to those for the unsubstituted parent compound. The next step is to understand the reason for this increase in internal conversion rate and this requires the help of quantum chemical calculations.
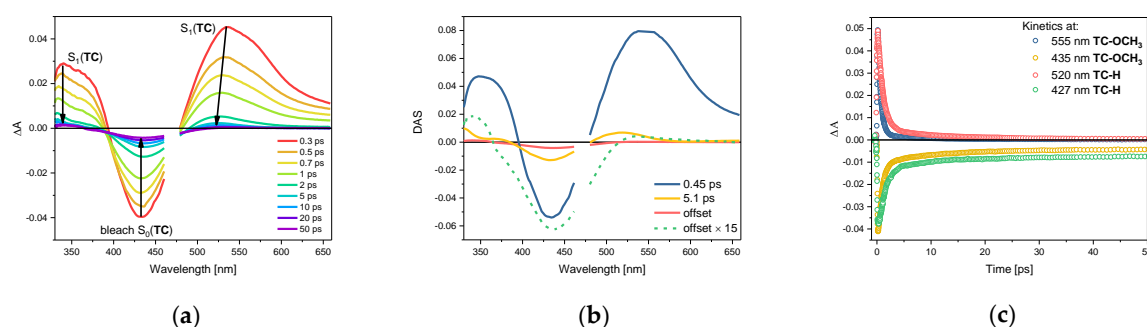
Figure 3. (**a**) Transient absorption UV-vis spectra recorded for TC-OCH$_3$ in cyclohexane (c $\approx 3 \times 10^{-4}$ M) upon excitation at 475 nm. (**b**) Global analysis shows decay associated spectra DAS with two time-constants 0.45 and 5.1 ps, and the offset. (**c**) Selected kinetic traces showing the TC S$_1$ state decay and TC S$_0$ repopulation. Data for TC-OCH$_3$ and TC-H were collected in the same experimental conditions.

2.4. Theoretical Modelling of TC→TT Photoisomerization Mechanism

In order to study the mechanism of the TC→TT photoisomerization reaction, it should be noted first that the molecular mechanism of rotation of the whole rotor unit vs. naphthalenone skeleton may be realized along the two different pathways (variations). They can be classified as *single-twist* or *bicycle-pedal* motion [30–34].

To visualize these two variations of the TC→TT photoisomerization process, the excited state (S$_1$) and ground-electronic state (S$_0$) two-dimensional minimum potential energy surfaces (S$_1$-PES, and S$_0$-PES, respectively) were constructed to compare the photoisomerization mechanism between the OCH$_3$ and H derivatives (see Figure 4). The molecule first evolves along the S$_1$-PES toward the region where the S$_1$→S$_0$ internal conversion process takes place (Figure 4a,b, for OCH$_3$ and H derivatives). Further evolution of the molecule follows the S$_0$-state gradient toward the stable minimum (Figure 4c,d). The PES minima of the ground state, S$_0$, and of the lowest excited state, S$_1$, were calculated using the MP2/cc-pVDZ and ADC(2)/cc-pVDZ methods, respectively. Each energy point at PES was obtained by optimization of the geometry of a given molecule imposing two constraints for driving coordinates: $\theta_1(C_{14} = C_1)$ and $\theta_2(C_2 = C_3)$, separately, in a given electronic state. These two driving coordinates were frozen while all the remaining 3N-8 coordinates were optimized for each point in given electronic state. Thus, each PES is spread over the two driving coordinates: $\theta_1(C_{14} = C_1)$ and $\theta_2(C_2 = C_3)$ (see Scheme 1, for definition) defined as the dihedral angles describing rotation about the respective double bond. Note also that the two phenyl rings in the rotor unit were distinguished and marked with letters: "a" and "b" in the molecular structure (see Scheme 1 and Figure 4) to discriminate between the *single-twist* and *bicycle-pedal* variant motions. In the excited state, the photoisomerization can be realized as the *single-twist* described as the rotation of the rotor unit vs. naphthalenone skeleton about the sole $C_{14} = C_1$ bond and could be observed along the direction parallel to the $\theta_1(C_{14} = C_1)$-axes in Figure 4a,b, for OCH$_3$ and H derivatives, respectively. The isomerization process, however, can be realized alternatively – as a *bicycle-pedal* motion – in which the concerted rotation about the two double bonds: $\theta_1(C_{14} = C_1)$ and $\theta_2(C_2 = C_3)$ takes place simultaneously. This movement can be seen as the two benzene rings: a and b moving in direction parallel to the naphthalenone moiety plane. The *bicycle-pedal* motion can be observed along the direction close to the diagonal of Figure 4a,b. It links upper-left and bottom-right corners of the respective S$_1$-PES so that the condition $\Delta\theta_1 = -\Delta\theta_2$ is approximately fulfilled.
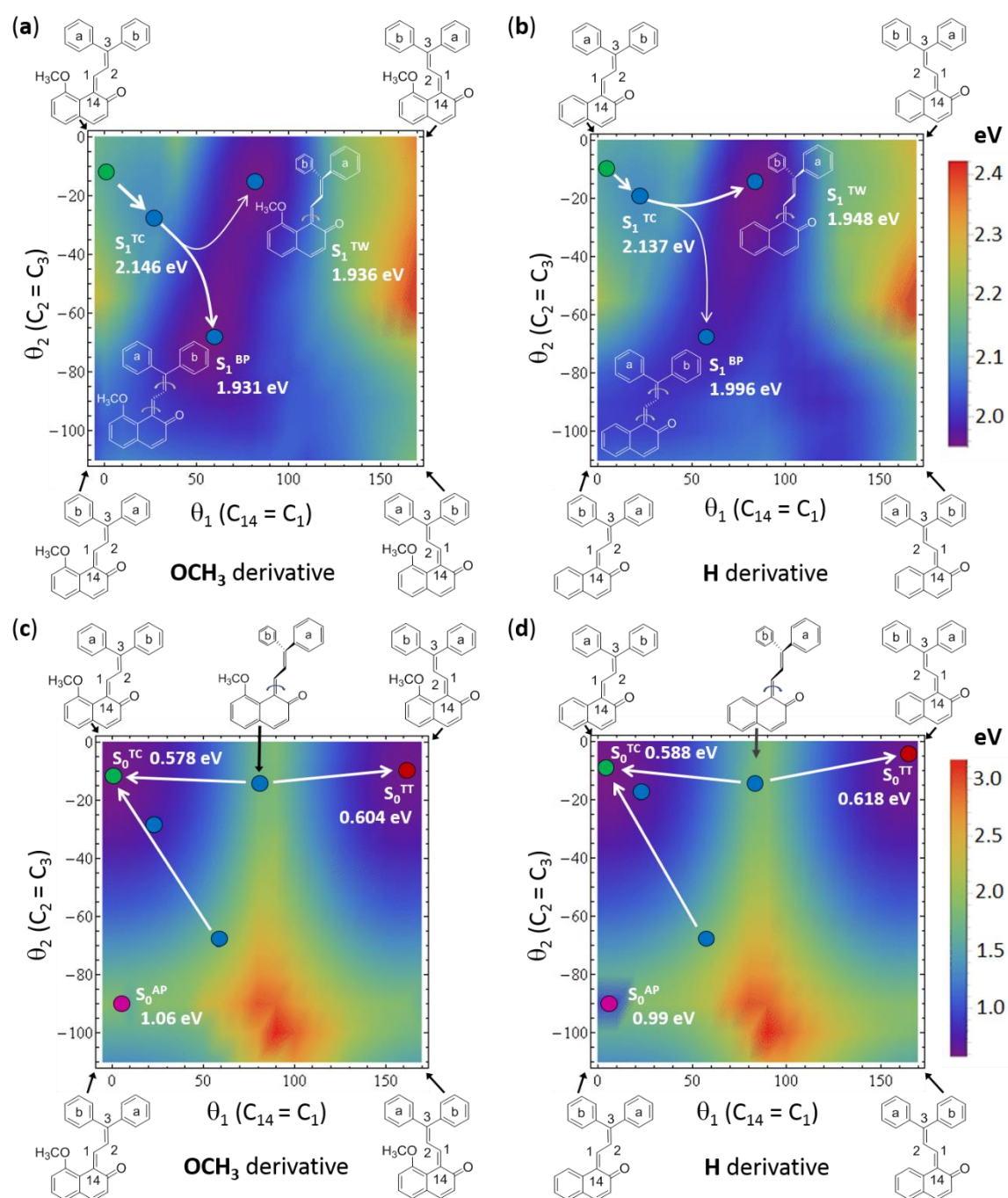
Figure 4. Minimum-potential-energy surface of the lowest excited electronic state (upper row, (**a**,**b**)) and the ground state (lower row, (**c**,**d**)) of H (right column) and its methoxy derivative (left column) plotted as a function of $\theta_1(C_{14} = C_1)$ and $\theta_2(C_2 = C_3)$ coordinates. The energy values at selected geometries are given in eV. Green, red and magenta circles represent the FC region of the ground-state S_0^{TC}, S_0^{TT}, and S_0^{AP} local minima, respectively. Blue circles represent various types of excited-state minima: S_1^{TC}—the minimum initially populated after S_0^{TC} photoexcitation, S_1^{BP}—achieved through the *bicycle-pedal* motion, and S_1^{TW}—reached by *single-twist* motion mechanism. Bold white arrows indicate the expected downhill motion of the wavepacket following the photoexcitation of TC form in its FC region. The results were obtained with the aid of the ADC(2)/cc-pVDZ method for the excited state and with the MP2/cc-pVDZ for the ground state.

Photoexcitation of TC isomer in its Franck-Condon region populates the $\pi\pi^*$ excited state. Next, the excited-state relaxation proceeds in a barrierless fashion from the TC Franck-Condon region toward the relaxed excited-state minimum, S_1(TC) form. As shown for the unsubstituted molecule [25], this relaxation process is accompanied by elongation of the $C_{13} = O_4$ carbonyl double bond which eventually becomes single and the excited state gains the $n\pi^*$ character. This mechanism resembles that discovered for DNA bases in which the $n\pi^*$ state is responsible for driving the system in the region of the conical intersection with the ground electronic state $CI(n\pi^*/S_0)$ [35,36]. Thus, the populated excited-state minimum S_1(TC) is observed in the ultrafast experiment with transient absorption detection (Figure 3). This molecule evolves further along a few deactivation channels [25], including the one that drives the molecule toward the TT photoproduct. A detail analysis of the mechanism of this process was possible thanks to the use of the calculated PES. The relevant species obtained as a result of the excited-state geometry evolution are shown in Figure 5 and Table 2.
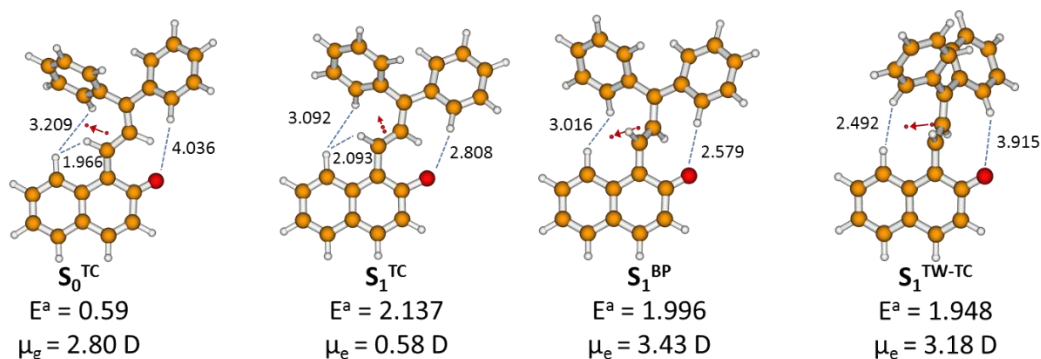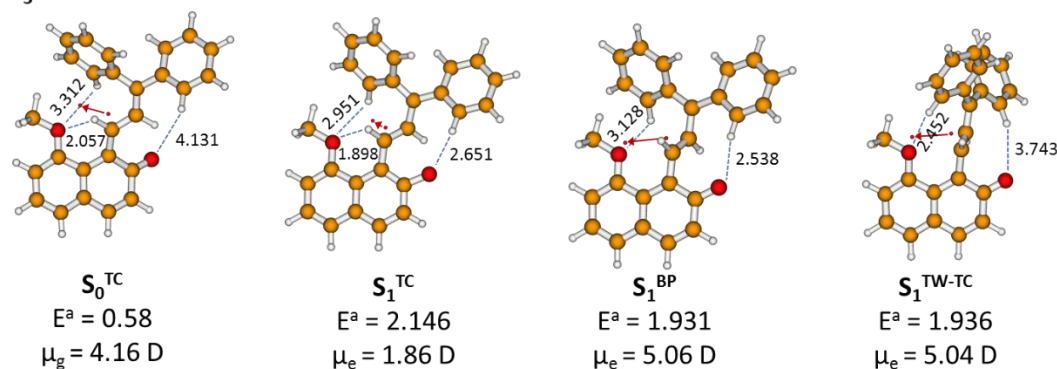

Figure 5. Considered ground and excited-state equilibrium geometries potentially involved in the TC→TT photoisomerization process of H (upper row) and OCH$_3$ (lower row) derivatives optimized at the MP2/cc-pVDZ(S$_0$) and ADC(2)/cc-pVDZ theory level. The corresponding intramolecular bond distances (in Å), adiabatic energy (E^a in eV), the dipole moment of the ground (μ_g, in D) and the excited-state form (μ_e, in D) are given.

Table 2. Comparison of geometric parameters (bond lengths, in Å, dihedral angles), adiabatic energies (E_a, in eV) for the excited state (S_1) geometries optimized at the ADC(2)/cc-pVDZ level of theory. σ and τ denote $C_{14}-C_1-C_2-C_3$ and $C_5-C_{13}-C_{14}-C_1$ dihedral angles, respectively.

S_0- or S_1-State Form	R_1 C_3-O_4 [Å]	θ_1 $C_{13}-C_{14}=C_1-C_2$ [°]	θ_2 $C_1-C_2=C_3-C_{15}$ [°]	σ [°]	τ [°]	R_2 $C_{13}-O_4$ [Å]	R_D C_1-C_{14} [Å]	R_S C_1-C_2 [Å]	R_E C_2-C_3 [Å]	E_a [eV]
			H-derivative							
S_0 TC	4.165	2.5	−9.5	173.5	160.3	1.239	1.386	1.437	1.384	0.59
S_1 TC	3.921	22.5	−18.7	−174.8	174.2	1.399	1.478	1.371	1.440	2.14
S_1 TW	4.433	84.7	−14.9	−170.0	180.0	1.266	1.474	1.366	1.445	1.95
S_1 BP	4.243	59.2	−68.5	−176.5	176.6	1.266	1.482	1.344	1.492	2.00
			OCH_3-derivative							
S_0 TC	4.086	1.8	−11.7	173.6	153.3	1.239	1.389	1.439	1.383	0.58
S_1 TC	3.818	25.5	−27.0	−174.9	172.8	1.390	1.483	1.364	1.450	2.15
S_1 BP	4.170	58.3	−69.1	−177.8	178.7	1.263	1.483	1.342	1.492	1.93
S_1 TW	4.308	82.6	−13.7	−177.2	177.3	1.260	1.476	1.366	1.439	1.94

We start our analysis of the process with the ground-state S_0^{TC} geometry whose position is marked with the green dot in the upper-left corner of Figure 4a,b, respectively, for methoxy and H derivatives. The single-photon excitation of S_0^{TC} form of each molecule in a barrierless manner populates the excited-state S_1^{TC} minimum. The first difference between the molecules occurs in the position of the S_1^{TC} minimum on the corresponding S_1-PES (blue dot in the upper left corner of Figure 4a,b).

During the initial S_1-state relaxation process of TC, both double bonds (θ_1, θ_2) become twisted from their initial Franck-Condon region values (1.8°, −11.7°), for $S_0^{TC}(OCH_3)$, down to (25.5°, −27°), for $S_1^{TC}(OCH_3)$ minimum; and from the initial values (2.5°, −9.5°), for $S_0^{TC}(H)$, down to (22.5°, −18.7°), for $S_1^{TC}(H)$ minimum (see Table 2). In case of the H derivative, the S_1^{TC} geometry points toward the *single-twist* motion path along the direction parallel to the $\theta_1(C_{14} = C_1)$-axis ($\theta_1 = 22.5°$, $\theta_2 = -18.7°$).

However, the $S_1^{TC}(OCH_3)$ geometry ($\theta_1 = 25.5°$, $\theta_2 = -27.0°$) lies much closer to the diagonal of the S_1-PES, where the $\theta_1 = -\theta_2$ *bicycle-pedal* condition is fulfilled. The S_1^{TC} form becomes an intermediate, whose geometry may determine further evolution of the molecule in the electronic excited state toward TT along the *single-twist* or *bicycle-pedal* pathway. These two mechanism variations populate a given type of the excited-state minimum: S_1^{BP}, for *bicycle-pedal*, or S_1^{TW}, for *single-twist* motion, respectively, shown in Figure 5.

For OCH_3 derivative (Figure 4a), the violet region forms a double minimum valley linking the two almost isoenergetic excited-state minimum geometries (blue dots): S_1^{BP} and S_1^{TW} separated by a very low energy barrier. S_1^{TW} [$\theta_1 = 82.6°$, $\theta_2 = -13.7°$] is located in the midpoint between the S_0^{TC} and S_0^{TT} geometries (green and red circles) illustrating t*wisting* motion of the molecule. The second minimum, S_1^{BP} [$\theta_1 = 58.3°$, $\theta_2 = -69.1°$], is located in the region close to the diagonal of Figure 4a suggesting that the *bicycle-pedal* mechanism should prevail over the *twisting* motion in the OCH_3 molecule, for the energy reasons.

The S_1^{BP} and S_1^{TW} minima were also determined for the unsubstituted parent compound. In this case, the S_1^{TW} excited-state global minimum [$\theta_1 = 84.7°$, $\theta_2 = -14.9°$] is more energetically favored. It is by 0.05 eV more stable than that of the corresponding S_1^{BP} form [$\theta_1 = 59.2°$, $\theta_2 = -68.5°$]. As a consequence, the position of the deeper twist-type S_1^{TW} global minimum on S_1-PES suggests that the *twisting* motion prevails over the *bicycle-pedal*, for the model of unsubstituted compound. Furthermore in agreement with recently reported experiments [25] we can also rationalize that the use of polar solvent is another way to control the equilibrium between *bicycle-pedal* and *single-twist* motion leading to the suppression of the TT formation in the H derivative. Indeed, in a polar solvent, the *bicycle-pedal* pathway will be favored over *single-twist* motion since the former path leads to a more polar intermediate S_1^{BP} (Figure 5), which likely produces back TC form after $S_1 \rightarrow S_0$ internal conversion. Moreover, in a polar solvent such as acetonitrile, the lifetime τ_{S_1} of TC is shorter in comparison to that in a non-polar cyclohexane (0.27 ps vs. 0.47 ps for OCH_3 derivative and 0.31 ps vs. 0.87 ps for H derivative, see Table 1) [25].

Even though after photoexcitation of TC-OCH_3 the excited-state gradient pulls the molecule toward the S_1^{BP} region, the S_1-state PES still indicates the existence of a low-lying flat energy valley reaching toward the region located around $\theta_2 = -90°$ (blue region on the lower-left part of Figure 4c,d). This is the region illustrating sole *single-twist* motion around the $C_2 = C_3$ double bond of the H and OCH_3 derivatives. During this alternative *twist* motion, the proton attached to the C_2 carbon atom in allene chain is found in vicinity of the carbonyl oxygen atom, O_4, that pulls the proton to form a stable AP minimum. The ground-state energy surface S_0-PES of both molecules indicates the existence of a high-energy ground-state equilibrium naphthalenol AP form (see the structure in Table S2). Depopulation of the excited state in this region may generate the AP form in the electronic ground state. The formation of the AP form has been detected in NMR studies for the TC-H molecule [8].

2.5. Role of the Methoxy Group

The π-electron-donating character of the methoxy group has been studied recently in both, ground- [37] and excited state [38] of monosubstituted benzenes. The electron donating effect of the

methoxy group is even greater in the excited S_1 state than in the S_0 state. The presence of a methoxy group in the species shown in Figure 5 results in a greater dipole moment of either the ground- or excited state due to a shift of electron-density from the methoxy group toward the carbonyl oxygen atom, O_4. The O_4 oxygen atom attracts phenyl b ring more in OCH_3 than in H derivative. It results in energetic stabilization of the corresponding excited-state species, S_1^{BP} and S_1^{TW}. In OCH_3 derivative, shortening of the C=O_4···H distance stabilizes the *bicycle-pedal* type excited-state species S_1^{BP} vs. the *single-twist* one. Thus, we claim here that the role of the methoxy group is mostly to shift electron density toward the carbonyl oxygen atom which attracts the whole rotor unit more strongly than in unsubstituted derivative. This strengthen attraction results in a slight tilt of the rotor toward the carbonyl group in all the structures in the singlet excited state (C_{10}-C_1 and C_{10}-C_2 distances increase by 0.1 Å). The electronic effect is affecting the photophysics of the process and is dominating over the steric effect caused by the incorporation of the relatively small methoxy group into the molecule. This thesis is supported by experimental finding that 10-bromo substituted compound photoproduces a similar TT yield as the H derivative [21]. However the steric effect with more bulky substituents needs further investigations.

The molecular system in the excited S_1 state can deactivate to the electronic ground state, S_0, through $S_1 \rightarrow S_0$ internal conversion. Thus, the ground state S_0-PES was constructed for both molecules (see Figure 4a,b, for H and OCH_3, respectively). The height of the S_0-state energy barrier precludes the TC→TT photoisomerization process to be thermally activated.

As one can see, the blue dot representing the geometry of *twisting* type excited-state S_1^{TW} minimum is located close to the top of the green region representing the S_0-state energy barrier for both molecules. The system after S_1-state deactivation follows the S_0-state energy gradient and eventually gains toward the TT photoproduct (S_0^{TT}), or goes back to TC form (S_0^{TC}).

In contrast to the twisting motion, the blue dot representing the *bicycle-pedal* type S_1^{BP} minimum is positioned on the left side of the S_0-state energy barrier. The deactivation of S_1^{BP} favors return of the system toward the ground-state TC form, since once being in the ground state, the molecule meets a high barrier for the TC→TT isomerization and the ground-state energy gradient pulls it back to TC isomer. Thus, the channel path populating the S_1^{BP} minimum may result in stopping the photoisomerization process. The *bicycle-pedal* motion in the S_1-state prevails over the *single-twist* for OCH_3 derivative, thus a lower TC→TT isomerization quantum yield for this molecule can be expected, which is in agreement with experimental finding.

3. Materials and Methods

3.1. Materials

CF-OCH_3 (10-methoxy-3,3-diphenyl-3*H*-benzo[*f*]chromene) was synthesized and purified accordingly to previously described procedures [21]. CF-H (3,3-diphenyl-3*H*-benzo[*f*]chromene) was purchased from TCI (Springfield, Virginia, USA).

3.2. Transient UV-Vis Absorption Spectra Over Seconds

UV LED (λ_{exc} = 365 nm, M365LP1, Thorlabs, Newton, New Jersey, USA) was used to perform photochromic reaction in a 1 cm × 1 cm fused silica cuvette placed in a temperature-controlled cuvette holder (Flash 300, Quantum Northwest, Liberty Lake, Washington, USA) with stirring (see Scheme S1). The volume of the solution was about 1.5 mL. Changes in UV-vis absorption spectra over seconds were recorded by a FLAME-T-VIS-NIR-ES USB spectrometer (6 s^{-1} sampling rate, Ocean Optics, Largo, Florida, USA). White-light of 150 W xenon lamp (Applied Photophysics, Leatherhead, Surrey, United Kingdom) with intensity reduced to a small level was used as a probing beam. 150 ms were used for accumulation of each white-light continuum spectrum. An average of 60 initial spectra before sample UV-irradiation was used to calculate $I_0(\lambda)$ spectrum, the next spectra $I(\lambda)$ at subsequent times were

measured upon or after UV-irradiation to determine the transient absorption spectra accordingly to formula: $\Delta A(\lambda) = \log \frac{I_0(\lambda)}{I(\lambda)}$.

In order to study influence of UV irradiation power on TT formation a V-550 spectrophotometer (Jasco, Hachioji-shi, Tokyo) equipped with the mentioned above temperature-controlled cuvette holder, stirring and UV LED source was used.

3.3. Transient UV-Vis Absorption Over Picoseconds

Femtosecond UV-vis transient absorption spectra were obtained using a commercially available system (Ultrafast Systems, Helios, Sarasota, Florida, USA) [39]. Photostationary state of TC was obtained by continuous UV irradiation (5 mW/cm^2) at 365 nm of CF solution in a quartz cell 2 mm thick with stirring.

The instrument response function (IRF) was about 200 fs (FWHM) estimated from a stimulated Raman scattering observed in pure solvent. The energy of laser pulses at 475 nm was 1 µJ. The data set was composed of a series of 280 spectra acquired for pump-probe delay ranging from -1 to 50 ps. Each transient absorption ΔA spectrum was calculated from 500 pairs of probe (pumpON) and reference (pumpOFF) spectra, it corresponded to 1 s of acquisition time (see Scheme S2). The obtained transient absorption spectra were analyzed using the global fitting procedure (ASUFIT program), satisfactory fits were obtained with a double-exponential function. Convolution with the instrument response function was included into the fitting procedure.

The accuracies of the obtained time-constants derived from analysis of transient absorption results were following: ± 5% (UV-vis data in time window over tens of seconds) and ± 10% (ultrafast UV-vis data).

3.4. Computational Details

The equilibrium geometries of the OCH$_3$ and H derivatives of 3*H*-naphthopyran and its isomers in their closed-shell ground state (S$_0$) were obtained with the MP2 method [40] without imposing any symmetry constrains. The energy of the most stable form CF is the reference energy for higher energy structures. The excited-state (S$_1$) equilibrium geometries were determined with the second-order algebraic diagrammatic construction ADC(2) method [41–43]. The correlation-consistent valence double zeta basis set with polarization functions on all atoms (cc-pVDZ) was used in these calculations as well as in potential energy surfaces [44]. The vertical excitation energies and response properties of the lowest excited singlet states were calculated using the ADC(2) and CC2 methods [45,46]. The aug-cc-pVDZ basis set augmented with the diffuse functions was also used to compute vertical excitation energies of the OCH$_3$ and H molecular system. All calculations were performed using TURBOMOLE program package [47].

4. Conclusions

The experiments in cyclohexane show TT photoreaction yield four times lower for methoxy derivative than for the parent unsubstituted compound. Ultrafast experiments demonstrated that the excited state lifetime τ_{S1} of TC-OCH$_3$ derivative is shorter (0.47 ± 0.05 ps) than that of TC-H (0.87 ± 0.09 ps) due to more effective radiationless S$_1$→S$_0$ internal conversion channel, populating back the TC form. Theoretical studies show two possible variants of photoisomerization reaction: (i) *single-twist* and (ii) *bicycle-pedal* motions. As demonstrated by the calculations, in photoexcited TC-OCH$_3$ the *bicycle-pedal* motion is energetically more favored than the *single-twist*. The *bicycle-pedal* motion leads to a minimum in S$_1^{BP}$ which is located in a close proximity of S$_0$-PES facilitating S$_1$→S$_0$ internal conversion, which through further structural evolution leads toward the relaxed TC minimum. The *bicycle-pedal* channel is less probable in H counterpart, which favors population of the single-twisted form S$_1^{TW}$. The excited-state decay of S$_1^{TW}$ leads to the ground state at the geometry close-lying to the S$_0$-state isomerization barrier, thus the energy gradient can drive the molecule toward TT or back to the TC minimum. Our studies have shown that the choice of appropriate substituent or polar solvent

can favor the *bicycle-pedal* TC→TT isomerization path, which can be aborted leading to the decrease in TT formation yield. Altogether, the *bicycle-pedal* path is seen as photostabilizing channel for TC form and opens the way to design new efficient naphthopyrans free from TT formation.

References

1. Becker, R.S.; Michl, J. Photochromism of synthetic and naturally occurring 2*H*-chromenes and 2*H*-pyrans. *J. Am. Chem. Soc.* **1966**, *88*, 5931–5933. [CrossRef]
2. Alberti, A.; Teral, Y.; Roubaud, G.; Faure, R.; Campredon, M. On the photochromic activity of some diphenyl-3*H*-naphtho[2, 1-*b*]pyran derivatives: Synthesis, NMR characterisation and spectrokinetic studies. *Dyes. Pigm.* **2009**, *81*, 85–90. [CrossRef]
3. Aubard, J.; Maurel, F.; Buntinx, G.; Poizat, O.; Levi, G.; Guglielmetti, R.; Samat, A. Femto/picosecond transient absorption spectroscopy of photochromic 3,3-diphenyl-naphtho[2,1-*b*]pyran. *Mol. Cryst. Liq. Cryst.* **2000**, *345*, 215–220. [CrossRef]
4. Coelho, P.J.; Carvalho, L.M.; Goncalves, L.F.F.F.; Silva, C.J.R.; Campos, A.M.; Gomes, M.J. Photochromic hybrid sol–gel films containing naphthopyrans. *J. Sol. Gel Sci. Technol.* **2010**, *56*, 203–211. [CrossRef]
5. Crano, J.C.; Flood, T.; Knowles, D.; Kumar, A.; Van Gemert, B. Photochromic compounds: Chemistry and application in ophthalmic lenses. *Pure Appl. Chem.* **1996**, *68*, 1395–1398. [CrossRef]
6. Crano, J.C.; Guglielmetti, R. *Organic Photochromic and Thermochromic Compounds: Main Photochromic Families*; Plenum Press: New York, NY, USA, 1999; Volume 1.
7. Delbaere, S.; Luccioni-Houze, B.; Bochu, C.; Teral, Y.; Campredon, M.; Vermeersch, G. Kinetic and structural studies of the photochromic process of 3*H*-naphthopyrans by UV and NMR spectroscopy. *J. Chem. Soc. Perkin Trans.* **1998**, *2*, 1153–1157. [CrossRef]
8. Delbaere, S.; Vermeersch, G. NMR characterization of allenyl-naphthol in the photochromic process of 3,3-diphenyl-[3*H*]-naphtho[2-1,*b*]pyran. *J. Photochem. Photobiol. A* **2003**, *159*, 227–232. [CrossRef]
9. Frigoli, M.; Maurel, F.; Berthet, J.; Delbaere, S.; Marrot, J.; Oliveira, M.M. The control of photochromism of [3*H*]-naphthopyran derivatives with intramolecular CH-π bonds. *Org. Lett.* **2012**, *14*, 4150–4153. [CrossRef]
10. Frigoli, M.; Mehl, G.H. Room temperature photochromic liquid crystal [3*H*]-naphtho[2,1-*b*]pyrans—photochromism in the mesomorphic state. *Chem. Commun.* **2004**, *18*, 2040–2041. [CrossRef]
11. Gentili, P.L.; Danilov, E.; Ortica, F.; Rodgers, M.A.J.; Favaro, G. Dynamics of the excited states of chromenes studied by fast and ultrafast spectroscopies. *Photochem. Photobiol. Sci.* **2004**, *3*, 886–891. [CrossRef]
12. Görner, H.; Chibisov, A.K. Photoprocesses in 2,2-diphenyl-5,6-benzo(2*H*)chromene. *J. Photochem. Photobiol. A* **2002**, *149*, 83–89. [CrossRef]
13. Hepworth, J.D.; Heron, B.M. Photochromic naphthopyrans. In *Functional Dyes*; Kim, S.H., Ed.; Elsevier: Amsterdam, The Netherlands, 2006; pp. 85–135.
14. Herzog, T.T.; Ryseck, G.; Ploetz, E.; Cordes, T. The photochemical ring opening reaction of chromene as seen by transient absorption and fluorescence spectroscopy. *Photochem. Photobiol. Sci.* **2013**, *12*, 1202–1209. [CrossRef] [PubMed]
15. Kumar, A. The relationship between the structure and the absorption spectra of naphtho[2,1-*b*]pyran. *Mol. Cryst. Liq. Cryst.* **1997**, *297*, 139–145. [CrossRef]
16. Liu, L.; Zhang, Y.; Wang, G.; Zhang, M.; Guan, H. High stability of photoinduced merocyanine in naphthopyran-doped polyvinylpyrrolidone electrospun nanofibers. *Polym. Int.* **2014**, *63*, 1991–1996. [CrossRef]

17. Ottavi, G.; Favaro, G.; Malatesta, V. Spectrokinetic study of 2,2-diphenyl-5,6-benzo(2*H*) chromene: A thermoreversible and photoreversible photochromic system. *J. Photochem. Photobiol. A* **1998**, *115*, 123–128. [CrossRef]

18. Pardo, R.; Zayat, M.; Levy, D. Thin film photochromic materials: Effect of the sol-gel ormosil matrix on the photochromic properties of naphthopyrans. *C. R. Chimie* **2010**, *13*, 212–226. [CrossRef]

19. Salemi-Delvaux, C.; Aubert, C.; Campredon, M.; Giusti, G.; Guglielmetti, R. On the photodegradation of 3,3-diphenyl-[3*H*]-naphtho[2,1-*b*]pyrane in solution: Mechanistic aspect. *Mol. Cryst. Liq. Cryst.* **1997**, *298*, 45–51. [CrossRef]

20. Zayat, M.; Levy, D. Photochromic naphthopyrans in sol–gel ormosil coatings. *J. Mater. Chem.* **2003**, *13*, 727–730. [CrossRef]

21. Inagaki, Y.; Kobayashi, Y.; Mutoh, K.; Abe, J. A simple and versatile strategy for rapid color fading and intense coloration of photochromic naphthopyran families. *J. Am. Chem. Soc.* **2017**, *139*, 13429–13441. [CrossRef]

22. Brazevic, S.; Sliwa, M.; Kobayashi, Y.; Abe, J.; Burdzinski, G. Disclosing whole reaction pathways of photochromic 3*H*-naphthopyrans with fast color fading. *J. Phys. Chem. Lett.* **2017**, *8*, 909–914. [CrossRef]

23. Moine, B.; Buntinx, G.; Poizat, O.; Rehault, J.; Moustrou, C.; Samat, A. Transient absorption investigation of the photophysical properties of new photochromic 3*H*-naphtho[2,1-*b*]pyran. *J. Phys. Org. Chem.* **2007**, *20*, 936–943. [CrossRef]

24. Moine, B.; Rehault, J.; Aloise, S.; Micheau, J.-C.; Moustrou, C.; Samat, A.; Poizat, O.; Buntinx, G. Transient absorption studies of the photochromic behavior of 3*H*-naphtho[2,1-*b*]pyrans linked to thiophene oligomers via an acetylenic junction. *J. Phys. Chem. A* **2008**, *112*, 4719–4726. [CrossRef] [PubMed]

25. Brazevic, S.; Baranowski, M.; Sikorski, M.; Rode, M.F.; Burdziński, G. Ultrafast dynamics of the transoid-*cis* isomer formed in photochromic reaction from 3*H*-naphthopyran. *ChemPhysChem* **2020**, *21*, 1402–1407. [CrossRef] [PubMed]

26. Arai, K.; Kobayashi, Y.; Abe, J. Rational molecular designs for drastic acceleration of the color-fading speed of photochromic naphthopyrans. *Chem. Commun.* **2015**, *51*, 3057–3060. [CrossRef] [PubMed]

27. Mutoh, K.; Kobayashi, Y.; Abe, J. Efficient coloration and decoloration reactions of fast photochromic 3*H*-naphthopyrans in PMMA-*b*-PBA block copolymer. *Dyes Pigm.* **2017**, *137*, 307–311. [CrossRef]

28. Brazevic, S.; Nizinski, S.; Szabla, R.; Rode, M.F.; Burdzinski, G. Photochromic reaction in 3*H*-naphthopyrans studied by vibrational spectroscopy and quantum chemical calculations. *Phys. Chem. Chem. Phys.* **2019**, *21*, 11861–11870. [CrossRef]

29. Van Gemert, B.; Kumar, A.; Knowles, D.B. Naphthopyrans. Structural features and photochromic properties. *Mol. Cryst. Liq. Cryst.* **1997**, *297*, 131–138. [CrossRef]

30. Gozem, S.; Luk, H.L.; Schapiro, I.; Olivucci, M. Theory and simulation of the ultrafast double-bond isomerization of biological chromophores. *Chem. Rev.* **2017**, *117*, 13502–13565. [CrossRef]

31. Redwood, C.; Bayda, M.; Saltiel, J. Photoisomerization of pre- and provitamin D3 in EPA at 77 K: One-bond-twist, not hula-twist. *J. Phys. Chem. Lett.* **2013**, *4*, 716–721. [CrossRef]

32. Saltiel, J.; Megarity, E.D.; Kneipp, K.G. The mechanism of direct cis-trans photoisomerization of the stilbenes. *J. Am. Chem. Soc.* **1966**, *88*, 2336–2338. [CrossRef]

33. Schapiro, I.; Weingart, O.; Buss, V. Bicycle-pedal isomerization in a rhodopsin chromophore model. *J. Am. Chem. Soc.* **2009**, *131*, 16–17. [CrossRef]

34. Warshel, A. Bicycle-pedal model for the first step in the vision process. *Nature* **1976**, *260*, 679–683. [CrossRef] [PubMed]

35. Hu, D.; Liu, Y.F.; Sobolewski, A.L.; Lan, Z. Nonadiabatic dynamics simulation of keto isocytosine: A comparison of dynamical performance of different electronic-structure methods. *Phys. Chem. Chem. Phys.* **2017**, *19*, 19168–19177. [CrossRef] [PubMed]

36. Perun, S.; Sobolewski, A.L.; Domcke, W. Conical intersections in thymine. *J. Phys. Chem. A* **2006**, *110*, 13238–13244. [CrossRef]

37. Ozimiński, W.P.; Dobrowolski, J.C. σ- and π-electron contributions to the substituent effect: Natural population analysis. *J. Phys. Org. Chem.* **2009**, *22*, 769–778. [CrossRef]

38. Dobrowolski, J.C.; Lipiński, P.F.J.; Karpińska, G. Substituent effect in the first excited singlet state of monosubstituted benzenes. *J. Phys. Chem. A* **2018**, *122*, 4609–4621. [CrossRef] [PubMed]

39. Wendel, M.; Nizinski, S.; Tuwalska, D.; Starzak, K.; Szot, D.; Prukala, D.; Sikorski, M.; Wybraniec, S.; Burdzinski, G. Time-resolved spectroscopy of the singlet excited state of betanin in aqueous and alcoholic solutions. *Phys. Chem. Chem. Phys.* **2015**, *17*, 18152–18158. [CrossRef] [PubMed]

40. Møller, C.; Plesset, M.S. Note on an aproximation treatment for many-electron systems. *Phys. Rev.* **1934**, *46*, 618–622. [CrossRef]

41. Hättig, C. Structure optimizations for excited states with correlated second-order methods: CC2 and ADC(2). *Advances in Quantum Chemistry* **2005**, *50*, 37–60.

42. Schirmer, J. Beyond the random-phase approximation: A new approximation scheme for the polarization propagator. *Phys. Rev. A* **1982**, *26*, 2395–2416. [CrossRef]

43. Trofimov, A.B. An efficient polarization propagator approach to valence electron excitation spectra. *J. Phys. B: At. Mol. Opt. Phys.* **1995**, *28*, 2299–2324. [CrossRef]

44. Dunning, T.H., Jr. Gaussian basis sets for use in correlated molecular calculations. I. The atoms boron through neon and hydrogen. *J. Chem. Phys.* **1989**, *90*, 1007–1023. [CrossRef]

45. Christiansen, O.; Koch, H.; Jørgensen, P. The second-order approximate coupled cluster singles and doubles model CC2. *Chem. Phys. Lett.* **1995**, *243*, 409–418. [CrossRef]

46. Hättig, C.; Weigend, F. CC2 excitation energy calculations on large molecules using the resolution of the identity approximation. *J. Chem. Phys.* **2000**, *113*, 5154–5161. [CrossRef]

47. TURBOMOLE, Version 7.1, a Development of University of Karlsruhe and Forschungszentrum Karlsruhe GmbH, 1989–2007. Since 2007 TURBOMOLE GmbH. Available online: http://www.turbomole.com (accessed on 10 June 2016).

Publisher's Note: MDPI stays neutral with regard to jurisdictional claims in published maps and institutional affiliations.